# Repeating Earthquakes with Remarkably Repeatable Ruptures on the San Andreas Fault at Parkfield

Rachel E. Abercrombie[1] (Boston University), Xiaowei Chen[2] and Jiewen Zhang[2]
[1]Boston University, Boston MA, USA; [2]University of Oklahoma, Oklahoma, USA

*For Submission to Geophysical Research Letters*

## Key Points

- All individual earthquakes in a repeating sequence at Parkfield exhibit identical directivity, unaffected by 2004 M6.
- One sequence (M~2.7) ruptures to the NW and one (M~2.5) to the SE, at ~0.8 × shear wave velocity
- Smallest magnitude sequences show most response to M6 earthquake but we cannot fully distinguish between path and source effects.

Corresponding Author:
Dr. Rachel E. Abercrombie
Department of Earth and Environment
Boston University
685 Commonwealth Avenue
Boston MA 02215
USA
Email: rea@bu.edu

## Abstract

We investigate the directivity of three well-recorded repeating sequences of earthquakes (M2-3, 2001 – 2016) on the San Andreas Fault at Parkfield (California) that are well-recorded by a borehole network.

We calculate rupture directivity and velocity from P waves using the empirical Green's function method. The individual events in each sequence all show the same directivity; those in the largest magnitude sequence (M~2.7, 8 events) rupture unilaterally to the NW (at ~0.8*Vs*), those in the second sequence (M~2.3, 9 events) rupture unilaterally to the SE, and those of smallest magnitude sequence (M~2, 11 events) are less well resolved.

The source spectra of the M~2.7 sequence exhibit no detectable temporal variation. The smaller M sequences both exhibit a decrease in high frequency energy following the M6 event, that recovers with time. This could be a consequence of a decrease in stress drop, an increase in attenuation, or a combination of the two, followed by gradual healing.

## Plain Language Summary

Sequences of small earthquakes with very similar seismograms have been observed on the San Andreas Fault at Parkfield, and many other faults that are also observed to be creeping. The similarity of the seismograms suggests that these earthquakes represent repeating slip on overlapping pieces of fault. Under this assumption they have been used to investigate changes in slip conditions, and the slip rate on major faults with time. To date, most studies have treated these repeating earthquakes as just points because most are too small and too poorly recorded to observe details of the rupture area or direction. Here we identify three exceptionally well recorded repeating sequences, and are able to resolve the direction of rupture. All the earthquakes in one sequence propagate towards the NW and all those in another propagate to the SW. The rupture velocities are similar to those of much larger earthquakes. This improved resolution of the earthquake sources will help constrain modeling of the rupture and hence our understanding of the factors that control earthquake nucleation and dynamics.

## Introduction

Repeating earthquakes were first identified on the San Andreas Fault system (Nadeau *et al.*, 1995; Vidale *et al.*, 1994), and have since been observed globally (Chen *et al.*, 2007; Uchida and

Bürgmann, 2019), typically on faults with long term creep; they are thought to involve rupture of isolated loaded patches that are surrounded by regions of ongoing aseismic slip. Analysis of repeating earthquakes has concentrated on relating the inter-event or recurrence time (*TR*) of the earthquakes to their seismic moment (defined as $M_0 = \mu AS$ where $\mu$ is rigidity, *A,* area of slip and *s*, slip) as these are relatively simple parameters to measure reliably for the numerous small magnitude sequences. The regular occurrence rates of individual sequences have been used to reveal temporal and spatial variation in fault creep rates (Peng *et al*., 2005; Chen *et al*., 2007; Uchida and Bürgmann, 2019). A large stress perturbation, such as a large nearby earthquake, causes the TR of repeating earthquake sequences (RES) to decrease dramatically, and then increase logarithmically, returning to the original background rate (Vidale *et al*., 1994; Chen *et al*., 2010; Peng *et al*., 2005) over a similar time scale to observed changes in post-seismic slip-rate (Freed, 2007), and velocity (Brenguier *et al*., 2008; Wu *et al*., 2016; Rubinstein and Beroza, 2005) and attenuation of the medium (Kelly *et al*., 2013). The seismic moments of some repeating events also change over the same time interval, with some sequences exhibiting increases, and others decreases (Chen *et al*., 2010; Peng *et al*., 2005; Uchida *et al*., 2015).

To relate the behavior of repeating earthquakes to slip rate and stress on the fault, and probe the factors controlling the earthquake nucleation and rupture process, requires separating the earthquake slip from the area. Earthquakes are known to have a relatively constant stress drop ($\propto$ $s/A^{1/2}$) from tiny laboratory acoustic emissions to great earthquakes (Abercrombie, 1995; Yoshimitsu *et al*., 2014). If earthquakes in RES also fit this relationship, then on a steadily creeping fault, we would expect $TR \propto s \propto M_0^{1/3}$, but observations show $TR \propto M_0^{1/6}$ (Nadeau *et al*., 1998; Chen *et al*., 2007). Dynamic modeling to explain this discrepancy shows that the earthquake rupture area must partially slip aseismically between events (Chen and Lapusta, 2009; Cattania and Segall, 2019), and enhanced dynamic weakening or elevated normal stress may be required in the source region (Lui and Lapusta, 2018). Reliable measurements of rupture area and slip in repeating earthquakes are relative rare, largely because of the scarcity of the high frequency, close-in recordings needed for analysis of such small earthquakes. Most studies of the occurrence rate of RES use the more numerous, and frequently occurring smaller magnitude sequences. To investigate the rupture processes of the largest (M~2.1) of the repeating earthquake sequences targeted by the San Andreas Fault Observatory at Depth (SAFOD), Dreger *et al*. (2007) and Kim *et al*. (2016) inverted the earthquake seismograms for slip distribution over a finite-fault plane. They revealed a roughly circular slip area, with a slightly larger area for the event following the 2004 M4, but the quantity and frequency content of the data required them to assume a rupture velocity and limited the constraints on the spatial variability of slip. Abercrombie (2014) estimated rupture area and stress drop for the three repeating earthquake sequences targeted by SAFOD, assuming a circular source model and constant rupture velocity. Abercrombie (2014) found that even using the borehole HRSN (High Resolution Seismic Network, HRSN, 2014) only earthquakes in the largest (M~2.1) RES could be resolved with any confidence, and that their stress drops fit within the ranges observed for non-repeating earthquakes. An immediate decrease in stress drop after the 2004 M6 earthquake, followed by gradual recovery was observed for this sequence (Abercrombie, 2014; Allmann and Shearer, 2007) and Chaves *et al*. (2020) resolve similar temporal behavior of stress drop for repeating sequences of earthquakes at the subduction interface at Nicoya, Costa Rica. These observations are consistent with simple relative measurements of spectral frequency content (Vidale *et al*., 1994; McLaskey *et al*., 2012) although these last could include temporal variation in attenuation. Ambiguity in distinguishing source and path effects (e.g. Abercrombie, 2015), and the assumption of a simplistic source model (Kaneko and Shearer, 2014; Lin and Lapusta, 2018) can lead to significant biases and uncertainties, although in the case of relatively simple sources that are well-recorded these issues are minimized.

Uchida *et al*. (2015), estimated the slip distribution for the larger (M~5) RES off Kamaishi, Japan, before and after the 2011 M9 Tohoku earthquake. They found overlapping rupture areas, (and average stress drops for events before the M9, Uchida *et al*., 2012) but the azimuthal range and distance to stations from the offshore RES location limited their resolution of directivity and rupture velocity. Similar limitations affected analysis of a quasi-periodic RES in Taiwan (Chen *et al*., 2016), that revealed overlapping rupture areas, but had negligible constraint on rupture velocity. The four events in the most periodic Taiwanese sequence all showed a similar rupture direction, suggesting a very repetitive rupture process. Relocation of the hypocenters of the Kamaishi sequence earthquakes before 2011, with respect to their centroids, also showed that they tend to nucleate in the SW of the source area (Uchida *et al*., 2012).

Modelling earthquakes as a line-source is an alternative approach to estimate rupture velocity and direction. It uses the azimuthal variation that is ignored when assuming a simple circular source model, but involves fewer unknowns than finite-fault (Dreger *et al*., 2007; Kim *et* *al.*, 2016) or even second moment inversion (McGuire, 2004). This makes it a good approach for analyzing data at the edge of the resolution threshold. Variations of the line-source approach have been applied to large numbers of small events on the San Andreas Fault system to investigate the hypothesis that contrasting rock properties on either side of a fault could control rupture direction (Lengliné and Got, 2011; Zhao *et al.*, 2010). There is a slight preference for rupture to the SE, but resolution is limited by their use of surface recordings; Wang *et al.* (2014) searched for earthquakes with clear evidence of directivity and was able to constrain their rupture velocity to be close to the shear wave speed, with considerable scatter.

Here we focus on exceptionally well-recorded RES occurring within the footprint of the HRSN (ensuring excellent azimuthal coverage) that have sufficiently large magnitude and duration to resolve the necessary detail, but are also small enough to have multiple repeats and not clip the borehole network recording system. The higher frequency signal recorded in the boreholes allows investigation of the source rupture at greater resolution than with the lower frequency surface data. We use an empirical Green's function approach to obtain source time functions and source spectra, and then use azimuthal and temporal variation to investigate the directivity and stress drops of events in the three sequences.

## Identification of Repeating Sequences

We use the relocated catalog for Northern California (NCAeqDD, Waldhauser and Schaff, 2008) to identify potential repeating earthquake sequences for detailed analysis. We search for earthquakes M ≥2, within the footprint of the HRSN that also have multiple repeats during the time of the current recording system of the HRSN (in operation since 2001; NCEDC, 2014), Figure 1.

Of the ten or so sequences that meet our initial criteria, most have few repeats, or include individual events that are poorly recorded. We identify 3 sequences suitable for detailed analysis, each including at least one event prior to the 2004 M6 Parkfield earthquake that was recorded by the current HRSN recording system. They are in order from NW to SE along the San Andreas Fault: Sequence 2: nearest to SAFOD, M~2.8, depth~3.9 km, 12 events, of which 8 recorded by current HRSN; Sequence 5: near to 1966 M6 hypocenter, M~2.0, depth~8.9 km, 17 events, of which we can analyze 11; and Sequence 9: M~2.5, depth~5.6 km, 14 events, of which we analyze 9 (Figure 2, Table S1).

Sequences 2 and 9 are relatively isolated, with no other sequences (or similar sized earthquakes) within a km, consistent with the results of Lui and Lapusta (2016). Sequence 5 is only ~0.5 km from a repeating sequence of relatively large, M~3.4 earthquakes with a recurrence interval of approximately 5 years. These larger events clip the nearby HRSN stations and so are not suitable for inclusion in the present study. They do not appear to have a significant effect on the timing of the earthquakes of Sequence; the 2004 M6 earthquake has a much larger effect on both sequences. Sequence 5 is also the only one of the 3 sequences within the slip-weakening zone used in the dynamic modeling of the Parkfield earthquake cycle by Barbot *et al.* (2012).

## Empirical Green's Function Analysis to Obtain Source Time Functions and Amplitude Spectra

We follow the procedures described by Abercrombie *et al.* (2017a), based on the approach developed by Abercrombie (2014), and use small earthquakes as empirical Green's functions (EGFs) to remove the path effects and calculate spectral ratios and relative source time functions (STFs) at each station for each earthquake (see SI). We find 73 EGFs for Sequence 2, 2 for Sequence 5 and 172 for Sequence 9 that meet our strict selection criteria (see SI and Table S1).

We deconvolve the EGF events from the main events (Prieto *et al.*, 2009) and obtain spectral ratios and source time functions (STFs) for each event at each station and component.

## Directivity

To measure the direction and speed of rupture requires quantifying the azimuthal variation in STF shape and duration (Figure 3). To avoid the need to pick start and end times of the STFs, which can be ambiguous, and to include the shape of the entire STF in the analysis, we use the stretching method developed by Prieto *et al.*, (2016) and Abercrombie *et al.* (2017b). We find the stretching coefficients that give the highest cross-correlation between STFs from an individual earthquake at all pairs of stations, and perform a grid search to find the orientation and velocity of a line source that best fits these coefficients. We calculate the take-off angles from the source using two 1D velocity models (one for stations to the NE of the fault and one to the SW) based on the model of Thurber *et al.* (2006). Following Abercrombie *et al.* (2017b), we try using a symmetrical bilateral line source, a purely unilateral line source, and also a line source that rupture twice as far in one direction to the other (2-to-1). Figures S2-S5 show examples of this fitting, and the results and misfits from the different models for all three sequences. The full 360° coverage provides excellent resolution of the direction of rupture, impossible for offshore earthquakes (Uchida *et al*., 2015).

The individual earthquakes in the two largest magnitude sequences (2 and 9) exhibit almost identical (within resolution, see Figure S1) azimuthal variation in STF shape and duration to the other events in the same sequence. We cannot resolve the difference between the purely unilateral and the 2-to-1 model, but Sequences 2 and 9 are significantly better fit with a more unilateral model than the symmetrical bilateral model. Their orientations and rupture velocities are well-resolved (Figure S5). All the earthquakes in Sequence 2 rupture to the NW and slightly up-dip, and all those in Sequence 9 to the SE (dip direction is less consistent, or well-constrained); the opposite directions are obvious from inspection of the azimuthal variation in STFs (Figure 3). The rupture direction of earthquakes in both sequences are unaffected by the M6 2004 earthquake. The earthquakes in Sequence 2 have the longest STFs with respect to the resolution limit, and so have the best resolved rupture velocity of 2-2.6 km/s (within 10% misfit of best model), ~0.8 $Vs$, where $Vs = S$ wave velocity. The earthquakes in Sequence 9 appear to have lower and more variable rupture velocity (~0.6-0.8 $Vs$ ), but this could be an artefact of the STFs being nearer the resolution limit, causing the rupture velocity to be under-estimated (Abercrombie *et al*., 2017b).

The STFs for Sequence 5 exhibit significantly less azimuthal variation and are equally well fit by the bilateral and unilateral models (Figure S5). Since their durations are only slightly longer than that of minimum resolution (a delta function with same sampling rate and filtering as the data, Figure S1) it is likely that we are not observing the real azimuthal variation and so cannot resolve the direction or rupture velocity. This is the same problem that limited the resolution of rupture velocity for the similar magnitude earthquakes targeted by SAFOD (Dreger *et al*., 2007; Kim *et al*., 2016).

## Temporal Variation in Earthquake Sources

The STFs of earthquakes in Sequence 2 and 9 show little evidence of temporal variation, but those in Sequence 5 are slightly longer for events immediately after the 2004 M6, suggesting an increase in rupture length (or a decrease in rupture velocity). This systematic decrease is clearer in the spectral ratios (Figure 4) which emphasize the higher frequency energy, and a temporal difference for Sequence 9 is also visible. These analyses use all available EGFs at all stations for each event, and so it is possible that variation between events within a sequence is an artefact of small variations in correction for each individual STF, and lack of correction for temporal variation in path effects (Kelly *et al*., 2015). We reanalyze the data using consistent sets of stations and EGFs, and also to allow for temporal variations.

The results using all available stations and EGFs, with no temporal separation are shown in Figures 3 and 4, and Figures S6 and S7 show the results when using the different EGF choices. Temporal variations in attenuation and EGFs are able to remove the minimal source variation of earthquakes in Sequence 2, and a significant part of the variation from those in Sequences 5 and 9. McLaskey *et al*. (2012) reported the strong response in frequency content of the earthquakes in Sequence 5 following the 2004 M6 earthquake, but they did not investigate in detail whether it could be an artefact of attenuation. Kelly *et al*. (2013) reported a strong immediate increase in attenuation following the M6, that gradually decayed to normal levels over 1-2 years, but their analysis assumed that there was no change in source parameters. A comparison of the results obtained here with different sets of EGFs and attenuation corrections confirms that either attenuation, or a combination of source and attenuation could be causing the temporal variation in frequency content. To resolve the ambiguity requires more events and more EGFs, better distributed in time to sample the rapid changes, than are available here.

## Source Parameters:

For comparison with previous studies, we model the spectral ratios using a simple circular source model, to obtain an estimate of the corner frequency and Brune-type stress drop (Brune, 1970). Since these earthquakes clearly exhibit unilateral rupture, and those in Sequence 2 involve multiple sub-events, the measurements are unlikely to be reliable as absolute measurements of stress drop. They do provide an estimate of the source dimension, and some quantification of the temporal variation, for comparison with events elsewhere. We follow the procedure developed by Abercrombie *et al*. (2017b) to model the spectral ratios calculated in the EGF analysis for source time functions, see SI. These ratios (Figure 4) are the spectra of the source time functions shown in Figure 3.

The results are shown in Figure S8, for all events with well-constrained fits. Most stress drops are in the typical range of ~5-50 MPa, and correspond to rupture dimensions of ~80 m,

~30m and ~50 m for Sequence 2, 5 and 9 earthquakes, respectively. Sequence 2 earthquakes have essentially constant stress drop and corner frequency within resolution. Sequence 5 shows a decrease in corner frequency and stress drop following the 2004 M6 event, indicating an increase in rupture area, then gradual recovery to pre-2004 levels. The corner frequencies of many earthquakes in this sequence were too high to be resolved within the bandwidth of the data – especially when only subsets of the EGFs were included, but the results reflect the temporal variation observed in the spectral ratios. The small number, and timing of the available EGFs prevents us from completely excluding the possibility that this is an artefact of temporal variation in attenuation. Sequence 9 shows a small decrease in corner frequency, following the 2004 M6 earthquake, for time-independent EGF selections, but this essentially disappears when correction for the time varying attenuation is included, suggesting that no resolvable change in source properties occurred.

## Discussion and Conclusions

The earthquakes in each of the two best resolved sequences studied here all start in a similar place, and rupture in the same direction at indistinguishable rupture velocity. These results are consistent with the indications of previous detailed studies (Chen *et al*., 2016; Lengliné and Got, 2011), although they lacked such good resolution. Our observations show that the rupture processes of repeating earthquakes can be remarkably repetitive.

Our best resolved rupture velocity measurements are ~0.8 *Vs*. These are consistent with those of larger earthquakes, and also for other well-recorded individual small earthquakes (Abercrombie *et al*., 2017b; Folesky *et al*., 2016). These measurements support assumptions used in previous spectral studies (Abercrombie, 2014; Allmann and Shearer, 2007; Abercrombie, 1995) and slip inversions (Dreger *et al*., 2007; Kim *et al*., 2016; Chen *et al*., 2016) of small repeating earthquakes. We choose line source models as they have the minimum number of unknowns needed to resolve the essential details of the sources. Alternative approaches such as second moment (inverting for orientation, velocity, length and width, e.g. McGuire, 2004) and finite fault slip inversions (also spatially varying slip, e.g. Kim *et al*., 2016) all involve significantly more unknowns and run the risk of losing clarity and resolution.

Why all the earthquakes in Sequence 2 rupture in the opposite direction to those in Sequence 9 presumably depends on the fault zone properties at the individual locations. Unfortunately, studies of velocity and attenuation structure at Parkfield do not have the resolution to observe variation on the scale of these source regions (Thurber *et al*., 2006; Zhao *et al*., 2010; Bennington *et al*., 2008); the different sequences could even be occurring on different fault strands within the system (Zoback *et al*., 2011).

Regardless, the consistency of rupture in successive earthquakes observed here implies that (for these sequences at least) the factors controlling rupture are remarkably stable. Surprisingly, the 2004 M6 earthquake did not affect either the direction of rupture, or the rupture velocity (within resolution limits) in any sequence. All three sequences studied here, though in regions with different rates of interseismic creep (Murray and Langbein, 2006), are so close to the regions of large slip in the M6 earthquake that it is likely the co-seismic slip passed through them; unfortunately slip of ~1 cm (typical of these M2-3 events) is below the resolution of coseismic and post-seismic slip inversions, so this cannot be confirmed (Murray and Langbein, 2006; Freed, 2007; Custódio *et al*., 2005; Hartzell *et al*., 2007; Barbot *et al*., 2012).

Repeating earthquakes are thought to result from small locked patches surrounded by regions of ongoing aseismic creep (Uchida and Bürgmann, 2019). Studies of fault zones, and dynamical modeling suggest various fault properties that could lead to localized weakening and earthquake nucleation within these locked patches; these include raised pore-pressure, increased normal stress, varying aseismic slip rates, heterogeneous stress distribution from the cumulative history of seismic and aseismic slip, and dynamic effects. The stability of the rupture process of these repeaters over multiple cycles, unaffected by the M6, suggests that geometry or material properties might be most likely candidates. For example, fault roughness is widespread and can lead to localized variation in normal stress (Griffith *et al*., 2010). Recent dynamic modeling work has focused on using the timing and seismic moment of earthquakes in RES to constrain frictional parameters (Lui and Lapusta, 2016; 2018) and these new observations provide useful further constraints. Determining the relative contributions of the various the controlling factors is a major component of physics-based earthquake dynamic modeling, the growing field aiming to improve forecasting of earthquake hazards (Lapusta *et al*., 2019).

Simple spectral modeling (Figure S8) reveals good agreement with previous estimates of stress drop for earthquakes at Parkfield (Abercrombie, 2014; Allmann and Shearer, 2007). Sequence 5 shows a decrease in corner frequency and stress drop following the 2004 M6 earthquake, similar to laboratory observations of slip (McLaskey *et al*., 2012). The decreased healing time and consequent fault zone weakening could increase the area, and decrease the slip and stress drop (e.g. Prieto *et al*., 2016; Chaves *et al*., 2020). However, the timing of the available EGFs cannot exclude the possibility this variation is an artifact of attenuation changes. Sequence 5 is close to the hypocenter of the 1966 M6 earthquake, where Allmann and Shearer (2007) observed a large increase in attenuation.

The smallest RES show most variation in seismic moment following a large event on the San Andreas Fault system (Chen *et al*., 2010), consistent with our observation of minimal, if any, response by the larger magnitude Sequences 2 and 9. The strong response of the M5 off-Kamaishi RES (Uchida *et al*., 2013) may be explained by the much greater stress perturbation caused by the 2011 M9 earthquake compared to the 2004 M6.

## Acknowledgements.

Funding for this work was provided by NSF Awards EAR 1547083 & 1547071. All data for this study come from the High Resolution Seismic Network (HRSN) doi:10.7932/HRSN, operated by the UC Berkeley Seismological Laboratory, which is archived at the Northern California Earthquake Data Center (NCEDC), doi: 10.7932/NCEDC.

## References

Abercrombie, R. E. (1995), Earthquake source scaling relationships from −1 to 5 $M_L$ using seismograms recorded at 2.5 km depth, *J. Geophys. Res*., **100**, 24,015– 24,036, doi:10.1029/95JB02397.

Abercrombie, R. E., 2014. Stress Drops of Repeating Earthquakes on the San Andreas Fault at Parkfield, *Geophys. Res. Lett., 41*, 8784–8791, doi:10.1002/2014GL062079.

Abercrombie, R. E., 2015. Investigating Uncertainties in Empirical Green's Function Analysis Earthquake Source Parameters, *J. Geophys. Res*., doi: 10.1002/2015JB011984.

Abercrombie, R. E., S. Bannister, J. Ristau, and D. Doser, 2017a. Variability of Earthquake Stress Drop in a subduction setting, the Hikurangi Margin, New Zealand, *Geophys. J. Int*., 208, 306-320, doi:10.1093/gji/ggw393.

Abercrombie, R. E., Poli, P. & Bannister, S. 2017b. Earthquake Directivity, orientation and stress drop within the subducting plate at the Hikurangi margin, New Zealand. *Journal of Geophysical Research: Solid Earth, 122*. https://doi.org/10.1002/2017JB014935

Allmann, B. P., and P. M. Shearer (2007), Spatial and temporal stress drop variations in small earthquakes near Parkfield, California, *J. Geophys. Res.*, **112**, B04305, doi:10.1029/2006JB004395.

Barbot, S., N. Lapusta and J.-P. Avouac (2012). Under the hood of the earthquake machine: Towards predictive modeling of the seismic cycle, Science, 336 (6082), 707–710, 2012, doi:10.1126/science.1218796.

Bennington, N., Clifford Thurber, Steve Roecker; Three-Dimensional Seismic Attenuation Structure around the SAFOD Site, Parkfield, California. *Bulletin of the Seismological Society of America* ; 98 (6): 2934–2947. doi: https://doi.org/10.1785/0120080175

Boatwright, J., 1980. A spectral theory for circular seismic sources: simple estimates of source dimension, dynamic stress drop, and radiated seismic energy, *Bull. Seism. Soc. Am. 70*, 1–28.

Brenguier, F., M. Campillo, C. Hadziioannou, N. M. Shapiro, R. M. Nadeau, E. Larose (2008). Postseismic Relaxation Along the San Andreas Fault at Parkfield from Continuous Seismological Observations, *Science*, 1478-1481.

Brune, J., (1970). Tectonic stress and the spectra of seismic shear waves from earthquakes, *J. Geophys. Res.*, *75*, 4997-5009.

Cattania, C., & Segall, P. (2019). Crack models of repeating earthquakes predict observed moment-recurrence scaling. Journal of Geophysical Research: Solid Earth, 124, 476– 503. https://doi.org/10.1029/2018JB016056

Chaves, E. J., S. Y. Schwartz & R. E. Abercrombie (2020). Repeating Earthquakes Record Fault Weakening and Healing Following a Megathrust Earthquake, *Science Advances, in press*.

Chen, K. H., Nadeau, R. M., and Rau, R.-J. (2007), Towards a universal rule on the recurrence interval scaling of repeating earthquakes? *Geophys. Res. Lett.*, 34, L16308, doi:10.1029/2007GL030554.

Chen, K. H., R. Bürgmann, R. M. Nadeau, T. Chen, and N. Lapusta (2010), Postseismic variations in seismic moment and recurrence interval of repeating earthquakes, *Earth Planet. Sci. Lett.*, **299**, 118– 125, doi:10.1016/j.epsl.2010.1008.1027.

Chen, K. H., Chen, I., and Kim, A. (2016), Can slip heterogeneity be linked to earthquake recurrence?, Geophys. Res. Lett., 43, 6916– 6923, doi:10.1002/2016GL069516.

Chen, T., and N. Lapusta (2009), Scaling of small repeating earthquakes, explained by interaction of seismic and aseismic slip in a rate and state fault model, *J. Geophys. Res.*, **114**, B01311, doi:10.1029/2008JB005749.

Custódio, S., Liu, P., and Archuleta, R. J. ( 2005), The 2004 $M_w$6.0 Parkfield, California, earthquake: Inversion of near-source ground motion using multiple data sets, *Geophys. Res. Lett.*, 32, L23312, doi:10.1029/2005GL024417

Dreger, D., R. M. Nadeau, and A. Chung (2007), Repeating earthquake finite source models: Strong asperities revealed on the San Andreas Fault, *Geophys. Res. Lett.*, **34**, L23302, doi:10.1029/2007GL031353.

Eshelby, J. D., 1957. The determination of the elastic field of an ellipsoidal inclusion and related problems, *Proc. Roy. Soc. Lond., A, 241*, 376-396.

Folesky, J., Kummerow, J., Shapiro, S. A., Häring, M., and Asanuma, H. ( 2016), Rupture directivity of fluid-induced microseismic events: Observations from an enhanced geothermal system, *J. Geophys. Res. Solid Earth*, 121, 8034– 8047, doi:10.1002/2016JB013078.

Freed, A. M. 2007), Afterslip (and only afterslip) following the 2004 Parkfield, California, earthquake, *Geophys. Res. Lett.*, 34, L06312, doi:10.1029/2006GL029155.

Griffith, W. A., Nielsen, S., Di Toro, G., and Smith, S. A. F. 2010), Rough faults, distributed weakening, and off-fault deformation, *J. Geophys. Res.*, 115, B08409, doi:10.1029/2009JB006925.

Hartzell, S., P. Liu, C. Mendoza, C. Ji, K. M. Larson (2007). Stability and Uncertainty of Finite-Fault Slip Inversions: Application to the 2004 Parkfield, California, Earthquake. *Bulletin of the Seismological Society of America* ; 97 (6): 1911–1934. doi: https://doi-org.ezproxy.bu.edu/10.1785/0120070080

HRSN (2014), High Resolution Seismic Network. UC Berkeley Seismological Laboratory. Dataset. doi:10.7932/HRSN.

Kaneko, Y., and P. M. Shearer (2014), Seismic source spectra and estimated stress drop from cohesive-zone models of circular subshear rupture, *Geophys. J. Int.*, doi:10.1093/gji/ggu030.

Kelly, C. M., A. Rietbrock, D. R. Faulkner, and R. M. Nadeau (2013), Temporal changes in attenuation associated with the 2004 M6.0 Parkfield earthquake, *J. Geophys. Res. Solid Earth*, **118**, 630– 645, doi:10.1002/jgrb.50088.

Kim, A., Dreger, D. S., Taira, T., and Nadeau, R. M. 2016), Changes in repeating earthquake slip behavior following the 2004 Parkfield main shock from waveform empirical Green's functions finite-source inversion, *J. Geophys. Res. Solid Earth*, 121, 1910– 1926, doi:10.1002/2015JB012562.

Lapusta, N., E. Dunham, J-P. Avouac, M. Denolle, Y. van Dinther, D. Faulkner, Y. Fialko, H. Kitajima, V. Lambert, S. Larochelle *et al*., 2019, Modeling Earthquake Source Processes: from Tectonics to Dynamic Rupture, Report to the National Science Foundation.

Lengliné, O., and Got, J.-L. (2011), Rupture directivity of microearthquake sequences near Parkfield, California, *Geophys. Res. Lett.*, 38, L08310, doi:10.1029/2011GL047303.

Lengliné, O., and Marsan, D. (2009), Inferring the coseismic and postseismic stress changes caused by the 2004 $M_w = 6$ Parkfield earthquake from variations of recurrence times of microearthquakes, *J. Geophys. Res.*, 114, B10303, doi:10.1029/2008JB006118.

Lin, Y.-Y., & Lapusta, N. 2018). Microseismicity simulated on asperity-like fault patches: On scaling of seismic moment with duration and seismological estimates of stress drops. *Geophysical Research Letters*, 45, 8145– 8155. https://doi.org/10.1029/2018GL078650

Lui, S. K. Y., & Lapusta, N. (2016). Repeating microearthquake sequences interact predominantly through postseismic slip. *Nat Commun* **7,** 13020, doi:10.1038/ncomms13020

Lui, S. K. Y., & Lapusta, N. (2018). Modeling high stress drops, scaling, interaction, and irregularity of repeating earthquake sequences near Parkfield. *Journal of Geophysical Research: Solid Earth*, 123, 10,854– 10,879. https://doi.org/10.1029/2018JB016472.

McGuire, J. J. (2004). Estimating finite source properties of small earthquake ruptures, *Bull. Seismol. Soc. Am.* 94, no. 2, 377–393.

McLaskey, G. C., A. M. Thomas, S. D. Glaser, and R. M. Nadeau (2012), Fault healing promotes high-frequency earthquakes in laboratory experiments and on natural faults, *Nature*, **491**, 101– 105, doi:10.1038/nature11512.

Murray, J., J. Langbein (2006). Slip on the San Andreas Fault at Parkfield, California, over Two Earthquake Cycles, and the Implications for Seismic Hazard. *Bulletin of the Seismological Society of America ; 96* (4B): S283–S303. doi: https://doi.org/10.1785/0120050820

Nadeau, R. M., W. Foxall, and T. V. McEvilly (1995), Clustering and periodic recurrence of microearthquakes on the San Andreas Fault at Parkfield, California, *Science*, **267**, 503– 507.

Nadeau, R. M., and L. R. Johnson (1998), Seismological studies at Parkfield VI: Moment release rates and estimates of source parameters for small repeating earthquake, *Bull. Seismol. Soc. Am.*, **88**, 790– 814.

Peng, Z., Vidale, J. E., Marone, C., and Rubin, A. 2005), Systematic variations in recurrence interval and moment of repeating aftershocks, *Geophys. Res. Lett.,* 32, L15301, doi:10.1029/2005GL022626.

Prieto, G. A., R. L. Parker, I F. L. Vernon, 2009. A Fortran 90 library for multitaper spectrum analysis, *Computers and Geosciences*, 35, 1701-1710, doi:10.1016/j.cageo.2008.06.007.

Prieto, G. A., B. Froment, C. Yu, P. Poli, and R. E. Abercrombie, 2016. Earthquake rupture below the brittle-ductile transition in continental lithospheric mantle, *Science Advances, 3, doi:10.1126/sciadv.1602642*.

Rubinstein, J. L., and G. C. Beroza (2005), Depth constraints on nonlinear strong ground motion from the 2004 Parkfield earthquake, Geophys. Res. Lett., 32, L14313, doi:10.1029/2005GL023189.

Rubinstein, J. L., Ellsworth, W. L., Chen, K. H., and Uchida, N. (2012), Fixed recurrence and slip models better predict earthquake behavior than the time- and slip-predictable models: 1. Repeating earthquakes, *J. Geophys. Res.*, 117, B02306, doi:10.1029/2011JB008724.

Shearer, P. M., Abercrombie, R. E., Trugman, D. T., & Wang, W. (2019). Comparing EGF methods for estimating corner frequency and stress drop from *P* wave spectra. *Journal of Geophysical Research: Solid Earth*, 124, 3966– 3986, https://doi.org/10.1029/2018JB016957

Thurber, C., H. Zhang, F. Waldhauser, J. Hardebeck, A. Michael, and D. Eberhart-Phillips (2006), Three-dimensional compressional wavespeed model, earthquake relocations, and focal mechanisms for the Parkfield, California, region, *Bull. Seismol. Soc. Am.*, **96**4B), S38– S49.

Uchida, N., T. Matsuzawa, W. L. Ellsworth, K. Imanishi, K. Shimamura, and A. Hasegawa (2012), Source parameters of microearthquakes on an interplate asperity off Kamaishi, NE Japan over two earthquake cycles, *Geophys. J. Int.*, **189**, 999– 1014, doi:10.1111/j.1365-246X.2012.05377.x.

Uchida, N., Shimamura, K., Matsuzawa, T., and Okada, T. (2015), Postseismic response of repeating earthquakes around the 2011 Tohoku-oki earthquake: Moment increases due to the fast loading rate, *J. Geophys. Res. Solid Earth*, 120, 259– 274, doi:10.1002/2013JB010933.

Uchida, N. and R. Bürgmann (2019), Repeating Earthquakes, Annual Review of Earth and Planetary Sciences 47:1, 305-332

Vidale, J. E., W. L. Ellsworth, A. Cole, and C. Marone (1994), Variations in rupture process with recurrence interval in a repeated small earthquake, *Nature*, **368**, 624– 626.

Waldhauser, F. and D.P. Schaff (2008), Large-scale relocation of two decades of Northern California seismicity using cross-correlation and double-difference methods, NCAeqDD v201112.1 *J. Geophys. Res.*, 113, B08311, doi:10.1029/2007JB005479.

Wang, E., Allan M. Rubin, Jean-Paul Ampuero, Compound earthquakes on a bimaterial interface and implications for rupture mechanics, Geophysical Journal International, Volume 197, Issue 2, May, 2014, Pages 1138–1153, https://doi.org/10.1093/gji/ggu047

Wu, C., Delorey, A., Brenguier, F., Hadziioannou, C., Daub, E. G., and Johnson, P. (2016), Constraining depth range of S wave velocity decrease after large earthquakes near Parkfield, California, *Geophys. Res. Lett., 43,* 6129– 6136, doi:10.1002/2016GL0691.

Yoshimitsu, N., Kawakata, H., and Takahashi, N. (2014), Magnitude −7 level earthquakes: A new lower limit of self-similarity in seismic scaling relationships, *Geophys. Res. Lett.,* 41, 4495– 4502, doi:10.1002/2014GL060306.

Zhao, P., Zhigang Peng, Zheqiang Shi, Michael A. Lewis, Yehuda Ben-Zion, (2010) Variations of the velocity contrast and rupture properties of M6 earthquakes along the Parkfield section of the San Andreas fault, Geophysical Journal International, Volume 180, Issue 2, Pages 765–780, https://doi.org/10.1111/j.1365-246X.2009.04436.x

Zoback, M., S. Hickman and W. Ellsworth, Scientific Drilling Into the San Andreas Fault Zone – An Overview of SAFOD's First Five Years, Scientific Drilling, 10.5194/sd-11-14-2011, 11, (14-28), (2011).

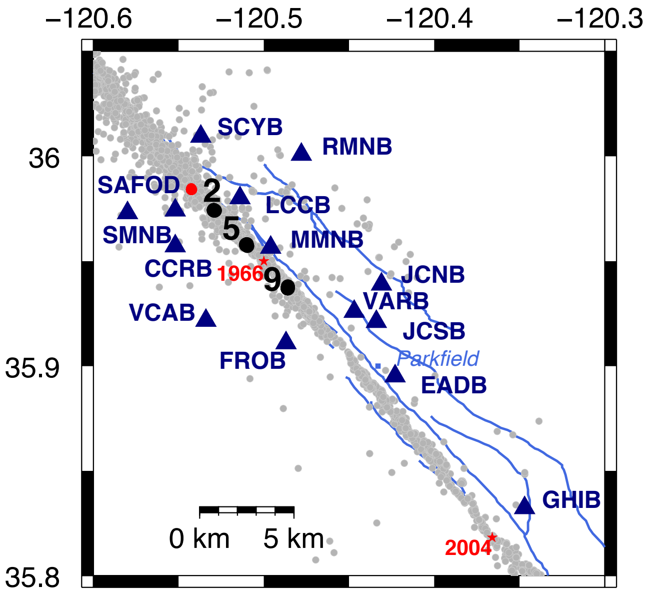


478 **Figure 1.** Location map of Parkfield, California showing the repeating sequences (2, 5 and 9) studied here (black circles), the SAFOD repeating sequence (red circles, origin in Figure 2, see SI Table), the HRSN stations and SAFOD Main hole (navy blue triangles), the background seismicity (grey circles[34]). The mapped faults (blue), M6 earthquake epicenters (red stars), and town of Parkfield (blue square) are also marked.

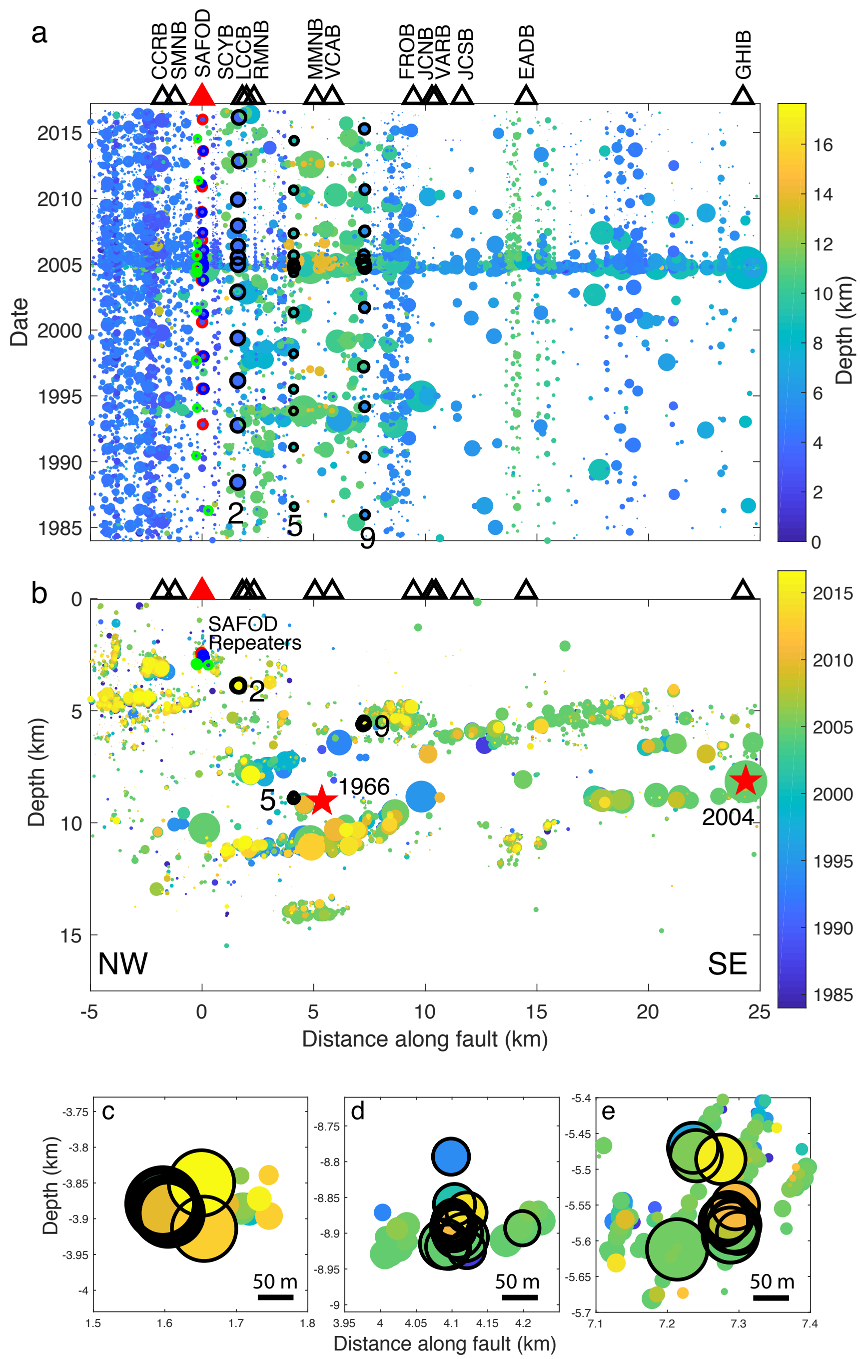


**Figure 2.** Identification of Repeating Earthquake Sequences. (a) Earthquakes on the San Andreas Fault as a function of time, along the fault, colored by their depth, size increases with magnitude. The SAFOD repeaters and the earthquakes in the three sequences studies here are highlighted. The HRSN stations are triangles; SAFOD is a red triangle. (b) Cross section of the San Andreas Fault showing the earthquakes colored by time, and size increases with magnitude. The SAFOD repeaters and the three sequences studied here are highlighted. The hypocenters of the 1996 and 2004 M6 earthquakes are shown as red stars. (c), (d) and (e) close ups from (b) of Sequences 2, 5 and 9, respectively.

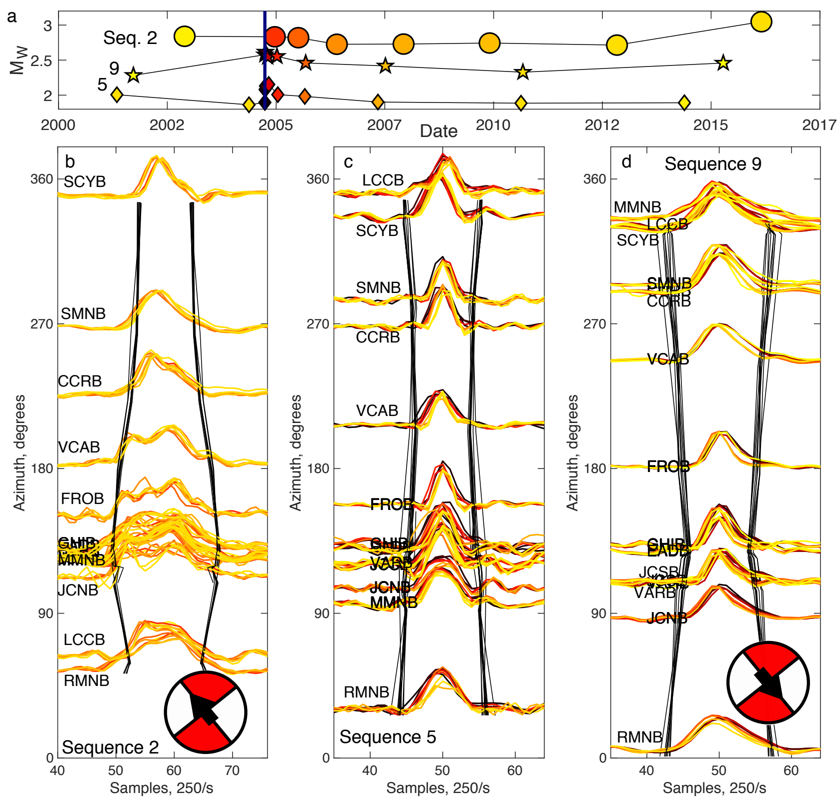


Figure 3

**Figure 3.** Source time functions for all earthquakes in the three sequences show consistent directivity. (a) Mw as a function of time for the three sequences, and provides a key to the colors used in (b), (c) and (d). The STFs for (b) Sequence 2, (c) Sequence 5 and (d) Sequence 9, are calculated using all available stations and EGFs, and colored by interevent time (*TR*) from dark (short) to yellow (long). Compare to Figure S6 for effects of EGF selection. STFs are normalized and plotted at the azimuth to the stations. The focal mechanisms show the direction of rupture for Sequences 2 and 9 along the San Andreas Fault. The black lines indicate the stretching predicted by the best fitting model to each event in each sequence, based on a median duration of the main pulse. Note the high consistency for Sequences 2 and 9. Sequence 5 exhibits greater variability between events and a smaller difference between stations, especially in the azimuth range 120 – 280 degrees.

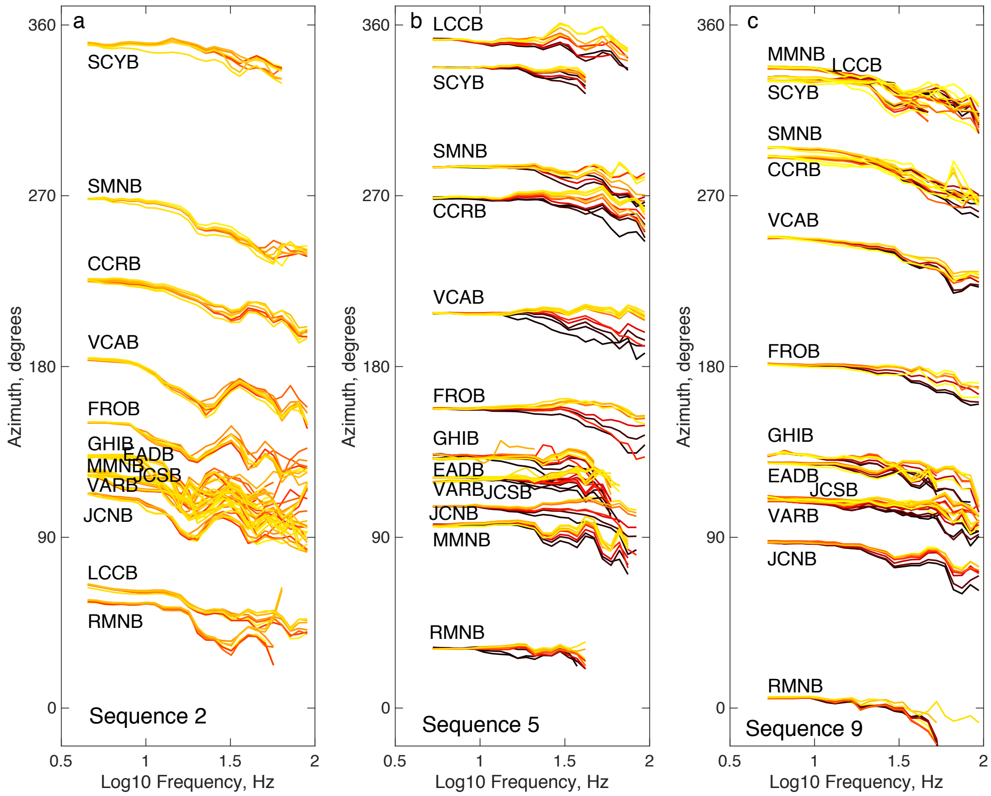


Figure 4

**Figure 4.** Spectral ratios for all earthquakes in the three sequences (a) 2, (b) 5, and (c) 9, corresponding to the source time functions in Figure 3; Coloring, stations and EGFs are the same as in Figure 3. The spectral ratios are normalized and plotted at the azimuth to the stations. The corner frequencies of the EGFs are above the maximum frequency. These ratios include no temporal variation in attenuation. Compare to Figure S7 for effects of EGF selection, and temporally varying attenuation with time. Note that the earthquakes with shortest repeat times have less high frequency energy than those with longer *TR*. Only the differences for Sequence 5 are consistently larger than any temporal correction for attenuation.